HHS Public Access

Author manuscript

J Am Soc Echocardiogr. Author manuscript; available in PMC 2022 April 01.

Published in final edited form as:

J Am Soc Echocardiogr. 2021 April ; 34(4): 433–442.e3. doi:10.1016/j.echo.2020.11.012.

ECHOCARDIOGRAPHIC MOLECULAR IMAGING OF THE EFFECT OF ANTI-CYTOKINE THERAPY FOR ATHEROSCLEROSIS

Weihui Shentu, M.D., Ph.D.[1], **Koya Ozawa, M.D., Ph.D.**[1], **TheAnh Nguyen, B.S.**[1], **Melinda D. Wu, M.D.**[2], **William Packwood, B.S.**[1], **Aris Xie, M.S.**[1], **Matthew A. Muller, B.S.**[1], **Eran Brown, M.S.**[1], **Matthew W. Hagen, Ph.D.**[1], **José A. López, M.D.**[3], **Jonathan R. Lindner, M.D.**[1,4]

[1]Knight Cardiovascular Institute, Oregon Health & Science University, Portland, Oregon

[2]Division of Pediatric Hematology and Oncology, Oregon Health & Science University, Portland, Oregon

[3]Bloodworks Research Institute, Seattle, Washington.

[4]Oregon National Primate Research Center, Oregon Health & Science University, Portland, Oregon

Abstract

Background: Echocardiographic molecular imaging techniques are beginning to be applied to evaluate pre-clinical efficacy of new drugs. In a large clinical trial, anti-IL-1β immunotherapy reduced atherosclerotic events, yet treatment effects were modest and the mechanisms of action were not fully elucidated. We tested the hypothesis that echocardiographic molecular imaging can assess changes in vascular thromboinflammatory status in response to anti-IL-1β therapy.

Methods: In wild-type and atherosclerotic mice deficient for the LDL-receptor and Apobec-1, closed-chest myocardial infarction (MI) was performed to mimic high-risk clinical cohorts. Control animals had sham-surgery. Post-MI animals were randomized to either no therapy or anti-IL-1β immunotherapy which was continued weekly. At post-MI day 3 or 21, *in vivo* ultrasound molecular imaging of aortic VCAM-1, P-selectin, von Willebrand factor (VWF) A1-domain, and platelet GPIbα in the thoracic aorta was performed. Aortic histology and NF-κB activity were assessed in atherosclerotic mice.

Results: In both atherosclerotic and wild-type mice, MI produced a several-fold increase ($p<0.05$) in aortic molecular signals for P-selectin, VCAM-1, VWF and GPIbα. In atherosclerotic mice, signal remained elevated at day 21. Anti-IL-1β therapy completely abolished the post-MI increase in signal for all endothelial targets ($p<0.05$ vs non-treated) at day 3 and 21. In atherosclerotic mice, MI triggered an increase in aortic plaque growth and macrophage content, a

Address correspondence to: Jonathan R. Lindner, MD, Knight Cardiovascular Institute, UHN-62, Oregon Health & Science University, 3181 SW Sam Jackson Park Rd., Portland, OR 97239, Tel. (503) 494-8750, Fax. (503) 494-8550, lindnerj@ohsu.edu.

DISCLOSURES

There are no conflicts of interest or other financial disclosures related to this work.

decrease in plaque collagen, and elevated aortic NF-κB ($p<0.05$ for all changes). All of these remote plaque adverse changes were inhibited by anti-IL-1β therapy.

Conclusions: Echocardiographic molecular imaging of the vascular endothelium can quantify the beneficial effects of therapies designed to suppress the pro-atherosclerotic arterial thromboinflammatory effects of alarmins such as IL-1β. This approach could potentially be used to evaluate the biologic variables that influence response in pre-clinical studies, and possibly to select patients most likely to benefit from therapy.

The innate immune response contributes to the development of atherosclerotic lesions and acute atherothrombotic events. The NLRP3 inflammasome pathway, including the caspase-mediated activation of interleukin-1β (IL-1β), has become a therapeutic target of large clinical trials. Inhibition of IL-1β reduces plaque development in mouse models of atherosclerosis.[1] In humans, the Canakinumab Anti-inflammatory Thrombosis Outcomes Study (CANTOS) demonstrated a reduction in events, especially recurrent myocardial infarction (MI), in high-risk patients treated with canakinumab, a monoclonal antibody against IL-1β.[2] Despite the ≈15% reduction in endpoints in CANTOS, the drug will apparently not receive regulatory approval for a cardiovascular application. Variability in treatment response was thought to influence this decision.

An important issue raised by CANTOS is whether efficacy of cytokine antagonism would be greatest in those who are at the highest risk of events. Risk assessment could be based either on clinical scenario or on laboratory values. In CANTOS, the magnitude of reduction in high-sensitivity C-reactive protein (CRP) identified those who benefitted the most from therapy,[3] yet this approach does not allow pre-treatment selection. Non-invasive imaging of the arterial thromboinflammatory processes or other markers of the "vulnerable vascular phenotype" that underlie acute coronary syndromes could be a more powerful way to meet the goals of precision medicine by either predicting those who are likely to benefit from new therapies, or demonstrating whether a patient is having the intended effect.[4,5] It could also be used to assess the relative efficacy of different drugs or doses in pre-clinical and clinical studies.[5] We hypothesized that *in vivo* echocardiographic molecular imaging would reveal suppression of arterial endothelial thromboinflammatory response by anti-IL-1β therapy in the post-MI setting. To test this hypothesis, we used targeted microbubble contrast agents to assess the global vascular activation response after myocardial infarction, schematically demonstrated in Figure 1. Specifically we imaged endothelial adhesion molecule expression and von Willebrand factor (VWF)- mediated platelet adhesion, all of which are thought to contribute to global plaque activation post-MI,[6] and are likely to be upregulated downstream to IL-1β pathways.

METHODS

Animal Models

The study was approved by the Animal Care and Use Committee of the Oregon Health & Science University. Wild-type C57Bl/6 mice, and double-knockout (DKO) mice with genetic deletion of both the low-density lipoprotein receptor and the Apobec-1 mRNA editing peptide were studied. The DKO strain develop reproducible, age-dependent atherosclerotic

aortic lesions on a chow diet, and were studied at 20-25 weeks-of-age when plaque size is modest.[7] Mice underwent closed-chest MI and were then randomized to either a control group or to receive a monoclonal antibody that inhibits murine IL-1β (401-NA, R&D Systems, Minneapolis, MN) (4 μg/g, I.P.) immediately before ischemia and on day 2, 4, 11, and 18 days after MI (Supplemental Figure 1). Sham-treated wild-type and DKO mice underwent preparation for closed chest MI but did not have ischemia-reperfusion performed. For all procedures, mice were anesthetized with 1.0% to 2.0% inhaled isoflurane, and a jugular vein was cannulated for intravenous access when required. Post-MI analgesia was performed with buprenorphine HCl (0.1 mg/kg subcutaneously).

Myocardial Infarction

A previously-described closed-chest model of MI was used to avoid acute inflammatory responses after thoracotomy and cardiac exposure.[6] At least 5 days prior to MI, mice were anesthetized, intubated, and placed on positive pressure mechanical ventilation with weight adjusted tidal volumes and respiratory rates. A limited left lateral thoracotomy was performed to expose only the basal anterior wall. A 8-0 nylon suture was place under the left anterior descending coronary artery but was left unsecured. The free ends of the suture were exteriorized through the chest wall and left in a subcutaneous location after closure. After 5-7 days, mice were anesthetized, the suture was exteriorized through a limited skin incision, and the tension was placed on the suture for 40 minutes to produce ST-segment elevation on electrocardiographic monitoring and wall motion abnormalities on high-frequency transthoracic 2 dimensional echocardiography (Vevo 2100, Visualsonic Inc., Toronto, Canada). Sham-treated animals received a suture without tightening.

Targeted Microbubble Preparation

Biotinylated lipid-shelled decafluorobutane microbubbles were prepared by sonication of gas-saturated aqueous lipid suspension of distearoylphosphatidylcholine (2 mg/mL), polyoxyethylene-40-stearate (1 mg/mL), and distearoylphosphatidylethanolamine-PEG (2000) biotin (0.4 mg/mL; Avanti Polar Lipids, Alabaster, AL). Surface conjugation of biotinylated ligands was performed as described previously using a streptavidin bridge.[7] Ligands used for targeting were: dimeric recombinant murine VWF A1 domain (mature VWF amino acids 445 to 716) for targeting platelet GPIbα;[6,8] a cell-derived biotinylated peptide representing the N-terminal 300 amino acids of GPIbα for targeting endothelial VWF;[8] and monoclonal antibodies against the extracellular domain of either P-selectin (RB40.34, BD Biosciences, San Jose, California), or VCAM-1 (clone 429, BD Biosciences). Control microbubbles were prepared with isotype control antibody (R3-34, BD Biosciences). Microbubble concentrations and size distributions were measured by eletrozone sensing (Multisizer III, Beckman Coulter).

Molecular Imaging

Echocardiographic molecular imaging was performed at either day 3 or 21 after MI, and at day 3 after sham-procedure. The ascending aorta and proximal aortic arch were imaged in the right parasternal window with a linear-array probe (Sequoia, Siemens Medical Systems, Mountain View, California). Multi-pulse imaging with phase-inversion and amplitude-modulation at 7 MHz was performed with a dynamic range of 55 dB and a mechanical index

of 1.0. Gain was set at a level that just eliminated pre-contrast background speckle and kept constant for all studies. Images were acquired 8 min after intravenous injection of targeted or control microbubbles (1×10^6 per injection), performed in random order. Signal from retained microbubbles alone was quantified, as previously described, by acquiring the first ultrasound frame and then digitally subtracting several averaged frames obtained after complete destruction of microbubbles at a mechanical index of 1.4 to eliminate signal from the low concentration of freely-circulating microbubbles in blood pool. Signal intensity was measured from a region-of-interest encompassing the entire ascending aorta to just beyond the origin of the brachiocephalic artery. Region selection was facilitated by fundamental 2-dimensional imaging at 14 MHz acquired after each imaging sequence.

Echocardiography

To detect any group-wise differences in infarct size or left ventricular function, high-frequency (30 MHz) transthoracic echocardiography was performed approximately 90 minutes after MI and at 10 days post-MI. Sham-treated mice were studied after a similar anesthesia time as in the 90 min studies. Images were obtained in a parasternal long-axis and parasternal short-axis planes at the basal, mid-LV, and apical imaging planes in order to calculate wall motion score index and measure LV dimensions at end-systole and end-diastole. Mid-ventricular fractional area change was measured from end-systolic and end-diastolic short-axis images. Stroke volume was calculated as the product of the LV outflow tract cross-sectional area and time-velocity integral on pulsed-wave Doppler using heel-toe angulation to reduce the angle of incidence on parasternal long-axis imaging, and angle corrected measurements.

Histology

Histology of the aortic root and the mid-ascending aorta for DKO mice was examined 21 days after MI using Masson’s trichrome for plaque area and collagen content, Mac-2 staining for macrophages, and CD41 staining for platelets (see Supplemental Methods).

Flow Cytometry

The presence of circulating platelet-leukocyte aggregates at day 3 post-MI was assessed by flow cytometry (see Supplemental Methods).

Arterial NF-κB

The aortic arch and descending thoracic aorta were removed from DKO mice at day 3 and 21 after MI, and at day 3 in sham-treated animals for measurement of NF-κB transcription factor complex p65 subunit (see Supplemental Methods).

Statistical Analysis.

Data analysis was performed with Prism version 8.0 (Graph Pad, La Jolla, California). Continuous variables that were normally distributed are displayed as mean±SEM, whereas those that were not normally distributed are displayed as box-whisker plots with a bar representing median, a box representing the interquartile range, and whiskers representing full range. Individual comparisons were made by Students’s t-tests (paired or unpaired) for

normally distributed data, and either a Mann-Whitney or Wilcoxon signed rank test was used as appropriate according to experimental conditions (group-wise comparisons versus paired data within a group). For multiple comparisons, a 1-way analysis-of-variance (ANOVA) was performed for normally distributed data with post-hoc testing with Holm-Sidak's multiple comparisons correction; whereas a Kruskal-Wallis test followed by Dunn's multiple comparison test were performed for non-normally distributed data.

RESULTS

LV Dimensions, LV Function, and Aortic Shear

Electrocardiographic ST-segment elevation and regional akinesis involving the LAD territory were observed in all mice at the time of closed-chest coronary artery ischemia, and were absent in animals undergoing sham surgical procedure. Compared to sham-treated controls, wild-type and DKO mice undergoing MI had larger LV end-diastolic and end-systolic dimensions at 90 minutes post-reperfusion (day 0), which persisted at day 10 post-MI (Figure 2A to 2D). Anti-IL-1β immunotherapy did not influence early or late post-MI LV dimensions. Reduced LV function in wild-type and DKO mice undergoing MI was manifested by a persistently lower fractional area change, lower stroke volume, and higher wall motion score index than sham controls (Figure 2E to 2J). Again there was no effect of anti-IL-1β therapy on these indices of LV function and segmental wall motion. These data indicate that neither mouse strain nor inhibition of IL-1β influenced the degree of LV dysfunction post-MI.

Post-MI Arterial Thromboinflammatory Activation

Echocardiographic molecular imaging was performed 3 days after MI in wild-type and DKO mice (Figure 3A to 3C). In either strain, mice undergoing MI compared to sham-treated controls demonstrated a several-fold higher degree of signal enhancement in the proximal thoracic aorta for endothelial VWF, platelet GPIbα, endothelial VCAM-1, and P-selectin. Signal enhancement from control non-targeted agent was low in sham-treated and post-MI groups. Treatment with anti-IL-1β immunotherapy after MI in either wild-type or DKO mice resulted in signal reduction for VWF, platelet GPIbα, VCAM-1, and P-selectin to a level similar to that seen in sham-treated animals. Because remote plaque activation by molecular imaging and secondary acceleration of plaque growth in DKO, but not wild-type, mice can persist for several weeks after MI,[6] molecular imaging was also performed at day 21 in post-MI DKO mice (Figure 3D). The selective signal enhancement for VWF, platelet GPIbα, endothelial VCAM-1, and P-selectin after MI was found to persist, whereas signal for control non-targeted agent remained low. The beneficial effects of inhibiting IL-1β with weekly administration of inhibitory antibody were sustained. Aortic NF-κB-P65, a pro-inflammatory transcription factor that is activated by IL-1β signaling and also contributes to IL-1β production by activating the NLRP3 inflammasome,[9] was increased in post-MI versus sham-treated DKO mice, and was significantly lower in post-MI animals treated with anti-IL-1β therapy (Supplemental Figure 2).

Plaque Morphology Post-MI

Plaque was observed only in DKO and not in wild-type mice. Examples of histology of the aortic root in post-MI DKO mice are illustrated in Figure 4. On quantitative analysis, plaque area assessed on Masson's trichrome-stained sections was significantly greater 21 days after MI compared to sham-treated controls (Figure 5A). The increase in plaque size post-MI was largely prevented in mice with anti-IL-1β therapy. The area staining for Mac-2 (Figure 5B), which includes plaque macrophages, was commensurate with group-wise differences in total plaque area; resulting in a similar percent of total plaque area that stained for Mac-2 (Figure 5C). In contrast, total plaque collagen remained relatively constant between groups (Figure 5D), despite the major differences in total plaque area. As a result, plaque collagen as a percentage of total plaque area was lower in post-MI versus sham-treated mice, except in those undergoing anti-IL-1β therapy (Figure 5E). Platelet CD41 staining was not observed in sham treated mice, whereas in post-MI mice staining was reduced by 98% in those treated with anti-IL-1β (Figure 5F). Together, the histology findings indicate that endothelial thromboinflammatory patterns seen on echocardiographic molecular imaging occurred in parallel with changes in plaque size and histologic markers of plaque risk.

Platelet-Leukocyte Aggregation

Platelet-leukocyte complexes are a component of systemic thromboinflammatory activation status, and could also represent an alternative or adjunctive mechanism to VWF for platelet adhesion. Accordingly, their presence in circulating blood was assessed by flow cytometry and defined by leukocyte-gated events with both CD45 and CD41 staining. The percentage of CD45-positive leukocytes that were coupled with platelets was significantly increased in post-MI versus sham-treated mice (Figure 6, Supplemental Figure 3). The post-MI increase in these complexes was inhibited by anti-IL-1β immunotherapy.

DISCUSSION

In patients with acute myocardial infarction or stroke, the ensuing several months is a vulnerable period when recurrent atherothrombotic event rate is high.[10] Enhanced risk applies not only to the infarct-related artery, but also to sites distant from the primary event. There have been many explanations for the increased global risk for events after MI. One established concept is that sudden ischemic events and cell death results in acute and often sustained release of systemic alarmins, an array of biomolecules that are part of the damage-associated molecular pattern network.[11] These compounds have downstream effects on the immune system, in part through inflammasome activation, and coagulation pathways operative in atherosclerosis,[11,12] representing a pathway for crosstalk between inflammation and platelets. By echocardiographic imaging of cellular and molecular events at the blood pool-endothelial interface, we have recently demonstrated that myocardial infarction can produce global endothelial activation both in large vessels and the microcirculation.[6] However, the mediators of this response have not been defined.

The main goal of the present study was to evaluate whether blockade of IL-1β prevents remote plaque activation following reperfused acute myocardial infarction. The study was conducted for two reasons. Firstly, the *in vivo* endothelial effects of anti-IL-1β therapy are

incompletely understood. The second reason was to establish that echocardiographic molecular imaging could be used as a tool for understanding and quantifying the relative efficacy of therapies designed to inhibit atherosclerosis, and alarmin pathways in particular. It can be surmised that imaging methods used successfully as a biologic readout of treatment effect could potentially be used in patient selection based on likelihood to benefit from therapy; and that this approach would be more specific than circulating markers of inflammation.

With regard to the mechanistic premise of the study, IL-1β is a potent cytokine implicated in a wide variety of inflammatory processes.[1] Its classical description is as an intermediate signal between the NLRP3 inflammasome and downstream pro-inflammatory and pro-coagulant effectors.[13] IL-1β has been shown to upregulate surface adhesion molecules, tissue factor, and VWF multimer production,[14] although most of these data are derived from *in vitro* models and cell culture preparations. Amplification of IL-1β effects can occur through multiple mechanisms. Endothelial expression of adhesion molecules and VWF leads to recruitment of leukocytes and platelets; both of which serve as a source of IL-1β.[15] Moreover, platelets have recently been shown to boost NLRP3 inflammasome activity and IL-1β production.[16] These mechanisms were among many others that were considered in the trial design of CANTOS.[1]

Our study was conducted in wild-type mice and a well-established genetic murine model of atherosclerosis caused by hyperlipidemia rich in human-like apolipoprotein-B100.[7] Administration of anti-IL1β was performed in a front-loaded fashion based on the early peak of IL1β and IL6 for several days after MI in mice.[17] We demonstrated that treatment with an antibody against murine IL-1β reduces early post-MI activation of endothelium remote from the coronary vasculature. Treatment effect was quantified by molecular imaging of adhesion molecules, endothelial-associated VWF in its active conformation (i.e. A1-domain accessibility), and platelet adhesion. In the atherosclerotic model, the effects of periodic administration of anti-IL-1β therapy was continued for several weeks based on previous studies showing that, while wild-type and DKO mice have a similar degree of remote vessel activation early post-MI, DKO have a much more prolonged duration of activation which likely contributes to accelerated plaque growth over the ensuing weeks.[6] Our results indicated that the beneficial effects of anti-IL-1β therapy on suppressing endothelial activation were sustained for several weeks. Anti-IL-1β therapy also suppressed NF-κB which is consistent with the prior research showing that this nuclear factor not only regulates IL-1β and NLRP3 transcription, but is also activated by IL-1β.[9,18] The effects of anti-IL-1β seen on molecular imaging and ELISA were associated with morphologic benefits. Therapy resulted in a marked blunting of the accelerated remote plaque growth and macrophage content ordinarily seen after MI.

This study is the first showing that *in vivo* molecular imaging with echocardiography can be used to assess endothelial effects produced by anti-IL-1β immunotherapy. Using microbubbles targeted to GPIbα, we demonstrated that the reduction in endothelial-associated VWF was associated with a reduction in platelet-endothelial adhesion. Previous studies have demonstrated the importance of endothelial-associated VWF multimers in platelet adhesion and plaque formation in murine atherosclerotic models.[19] Accordingly, we

believe VWF is an important contributor to thromboinflammation and our results indicate it is modifiable by inhibiting IL-1β. Because both pro-inflammatory leukocyte subsets and platelets express the IL-1R1 receptor, thereby permitting IL-1β auto-activation, it is likely that the endothelium is not the sole target for reducing thromboinflammatory activation by anti-IL-1β. This notion is supported by the reduction in platelet-leukocyte complexes found in our study. While we did not show explicitly that pre-therapy molecular imaging signal predicts treatment response, the group-wise patterns that link early molecular imaging signal (day 3) and plaque characteristics several weeks later provide evidence that molecular imaging of vascular phenotype can predict atherosclerotic course.

There are several limitations of the study that should be highlighted. First, there are important differences between mice and humans with regard to the progression and mediators of atherosclerosis. Most importantly, the mechanisms for remote plaque endothelial activation that we have defined in mice have not been fully studied in humans. However, remote plaque activation in humans has been suggested by studies showing higher ^{18}F-fluorodeoxyglucose signal on positron emission tomography in the carotid artery of patients with recent MI versus those with stable angina.[20] While we have demonstrated that anti-IL-1β therapy reduces both endothelial activation and plaque progression, we have not proven conclusively a causative link between the two. Instead, we must rely on the strong scientific evidence showing that inhibition of endothelial adhesion molecules and endothelial-platelet adhesion suppresses plaque progression. The study design which included pre-treatment of mice with anti-IL-1β therapy would seem to be contrary to clinical reality. However, administration was by I.P. route which requires up to 10 hours for intended plasma concentration to be reached.[21] While one would expect anti-IL-1β therapy to decrease post-MI LV remodeling, we did not find this to be the case. This finding is not entirely unexpected based on the mixed results found in murine, with studies showing both beneficial and adverse effects of anti-IL-1β therapy on remodeling.[22,23]

In summary, we have used echocardiographic molecular imaging of a broad array of vascular targets to demonstrate that a murine analog to canakinumab is capable of attenuating the atherothrombotic effects of remote endothelial activation after MI in wild-type and atherosclerotic mice. Our results contribute to the understanding of the biologic underpinnings of anti-cytokine therapy, and identify several thromboinflammatory processes involving the endothelium. Our data also suggest that echocardiographic molecular imaging could be used as a preclinical asset for proof-of-concept studies, or those performed to evaluate the drug or biologic variables that influence clinical response. Further studies are needed to determine whether molecular imaging patterns can also play a role in identifying likelihood of response to therapies designed to inhibit cytokines, alarmins, or other mediators of plaque activation.

Supplementary Material

Refer to Web version on PubMed Central for supplementary material.

Acknowledgments

SOURCES OF FUNDING

This work was supported by NIH grants R01-HL078610, R01-HL130046, and P51-OD011092 to Dr. Lindner; K08-HL133493 to Dr. Wu; and R35-HL145262 to Dr. Lopez. Dr. Lindner is also supported by grant 18-18HCFBP_2-0009 from NASA. Dr. Ozawa is supported by the JSPS Overseas Research Fellowship and Manpei Suzuki Diabetes Foundation. The work was also supported by AHA pre-doctoral grants 18PRE33960532 to Mr. Brown, and 20PRE35080066 to Mr. Nguyen.

REFERENCES

[1]. Libby P Interleukin-1 Beta as a Target for Atherosclerosis Therapy: Biological Basis of CANTOS and Beyond. J Am Coll Cardiol. 2017;70:2278–89. [PubMed: 29073957]

[2]. Ridker PM, Everett BM, Thuren T, MacFadyen JG, Chang WH, Ballantyne C, et al. Antiinflammatory Therapy with Canakinumab for Atherosclerotic Disease. N Engl J Med. 2017;377:1119–31. [PubMed: 28845751]

[3]. Ridker PM, MacFadyen JG, Everett BM, Libby P, Thuren T, Glynn RJ, et al. Relationship of C-reactive protein reduction to cardiovascular event reduction following treatment with canakinumab: a secondary analysis from the CANTOS randomised controlled trial. Lancet. 2018;391:319–28. [PubMed: 29146124]

[4]. Ridker PM. Clinician's Guide to Reducing Inflammation to Reduce Atherothrombotic Risk: JACC Review Topic of the Week. J Am Coll Cardiol. 2018;72:3320–31. [PubMed: 30415883]

[5]. Lindner JR, Link J. Molecular Imaging in Drug Discovery and Development. Circ Cardiovasc Imaging. 2018;11:e005355. [PubMed: 29449411]

[6]. Moccetti F, Brown E, Xie A, Packwood W, Qi Y, Ruggeri Z, et al. Myocardial Infarction Produces Sustained Proinflammatory Endothelial Activation in Remote Arteries. J Am Coll Cardiol. 2018;72:1015–26. [PubMed: 30139430]

[7]. Kaufmann BA, Carr CL, Belcik JT, Xie A, Yue Q, Chadderdon S, et al. Molecular imaging of the initial inflammatory response in atherosclerosis: implications for early detection of disease. Arterioscler Thromb Vasc Biol. 2010;30:54–9. [PubMed: 19834105]

[8]. Ozawa K, Packwood W, Varlamov O, Qi Y, Xie A, Wu MD, et al. Molecular Imaging of VWF (von Willebrand Factor) and Platelet Adhesion in Postischemic Impaired Microvascular Reflow. Circ Cardiovasc Imaging. 2018;11:e007913. [PubMed: 30571316]

[9]. He Y, Hara H, Nunez G. Mechanism and Regulation of NLRP3 Inflammasome Activation. Trends Biochem Sci. 2016;41:1012–21. [PubMed: 27669650]

[10]. Stone GW, Maehara A, Lansky AJ, de Bruyne B, Cristea E, Mintz GS, et al. A prospective natural-history study of coronary atherosclerosis. N Engl J Med. 2011;364:226–35. [PubMed: 21247313]

[11]. Fang L, Moore XL, Dart AM, Wang LM. Systemic inflammatory response following acute myocardial infarction. J Geriatr Cardiol. 2015;12:305–12. [PubMed: 26089856]

[12]. Roh JS, Sohn DH. Damage-Associated Molecular Patterns in Inflammatory Diseases. Immune Netw. 2018;18:e27. [PubMed: 30181915]

[13]. Loppnow H, Libby P. Proliferating or interleukin 1-activated human vascular smooth muscle cells secrete copious interleukin 6. J Clin Invest. 1990;85:731–8. [PubMed: 2312724]

[14]. Bevilacqua MP, Pober JS, Wheeler ME, Cotran RS, Gimbrone MA Jr. Interleukin-1 activation of vascular endothelium. Effects on procoagulant activity and leukocyte adhesion. Am J Pathol. 1985;121:394–403. [PubMed: 3878084]

[15]. Lindemann S, Tolley ND, Dixon DA, McIntyre TM, Prescott SM, Zimmerman GA, et al. Activated platelets mediate inflammatory signaling by regulated interleukin 1beta synthesis. J Cell Biol. 2001;154:485–90. [PubMed: 11489912]

[16]. Rolfes V, Ribeiro LS, Hawwari I, Bottcher L, Rosero N, Maasewerd S, et al. Platelets Fuel the Inflammasome Activation of Innate Immune Cells. Cell Rep. 2020;31:107615. [PubMed: 32402278]

[17]. Sager HB, Heidt T, Hulsmans M, Dutta P, Courties G, Sebas M, et al. Targeting Interleukin-1beta Reduces Leukocyte Production After Acute Myocardial Infarction. Circulation. 2015;132:1880–90. [PubMed: 26358260]

[18]. Hiscott J, Marois J, Garoufalis J, D'Addario M, Roulston A, Kwan I, et al. Characterization of a functional NF-kappa B site in the human interleukin 1 beta promoter: evidence for a positive autoregulatory loop. Mol Cell Biol. 1993;13:6231–40. [PubMed: 8413223]

[19]. Gandhi C, Ahmad A, Wilson KM, Chauhan AK. ADAMTS13 modulates atherosclerotic plaque progression in mice via a VWF-dependent mechanism. J Thromb Haemost. 2014;12:255–60. [PubMed: 24261607]

[20]. Kim EJ, Kim S, Kang DO, Seo HS. Metabolic activity of the spleen and bone marrow in patients with acute myocardial infarction evaluated by 18f-fluorodeoxyglucose positron emission tomograpic imaging. Circ Cardiovasc Imaging. 2014;7:454–60. [PubMed: 24488982]

[21]. Wahl RL, Barrett J, Geatti O, Liebert M, Wilson BS, Fisher S, et al. The intraperitoneal delivery of radiolabeled monoclonal antibodies: studies on the regional delivery advantage. Cancer Immunol Immunother. 1988;26:187–201. [PubMed: 3383203]

[22]. Hwang MW, Matsumori A, Furukawa Y, Ono K, Okada M, Iwasaki A, et al. Neutralization of interleukin-1beta in the acute phase of myocardial infarction promotes the progression of left ventricular remodeling. J Am Coll Cardiol. 2001;38:1546–53. [PubMed: 11691538]

[23]. Harouki N, Nicol L, Remy-Jouet I, Henry JP, Dumesnil A, Lejeune A, et al. The IL-1beta Antibody Gevokizumab Limits Cardiac Remodeling and Coronary Dysfunction in Rats With Heart Failure. JACC Basic Transl Sci. 2017;2:418–30. [PubMed: 30062160]

HIGHLIGHTS

- Echocardiographic molecular imaging is a valuable asset for pre-clinical assessment of new drugs targeted to atherosclerosis.
- Beneficial vascular anti-inflammatory and anti-thrombotic effects of anti-cytokn can be evaluated by echocardiographic molecular imaging.
- There is a role of echocardiographic molecular imaging for better understanding of new anti-atherosclerotic therapies, and possibly for selection of patients for drug trials.

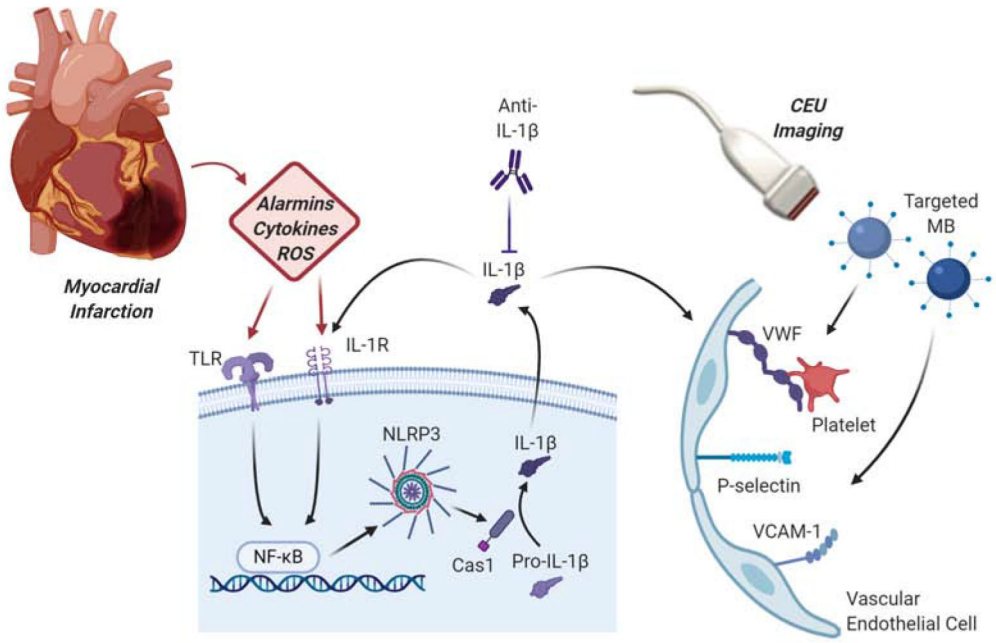

Figure 1.

Schematic illustrating the study design. Myocardial infarction results in damage-associated molecular patterns, which include alarmins, cytokines and reactive oxygen species (*ROS*). These compounds act with inflammatory cell receptors including toll-like receptors (*TLR*) and cytokine receptors such as IL-1R with downstream sequential activation of NF-κB and the NLRP3 inflammasome. NLRP3 activation of caspase 1 (*Cas1*) results in formation of IL-1β which then activates vascular endothelial cells to express VCAM-1, selectins, and endothelial-associated VWF multimers to which platelets adhere. CEU, contrast-enhanced ultrasound; MB, microbubbles.

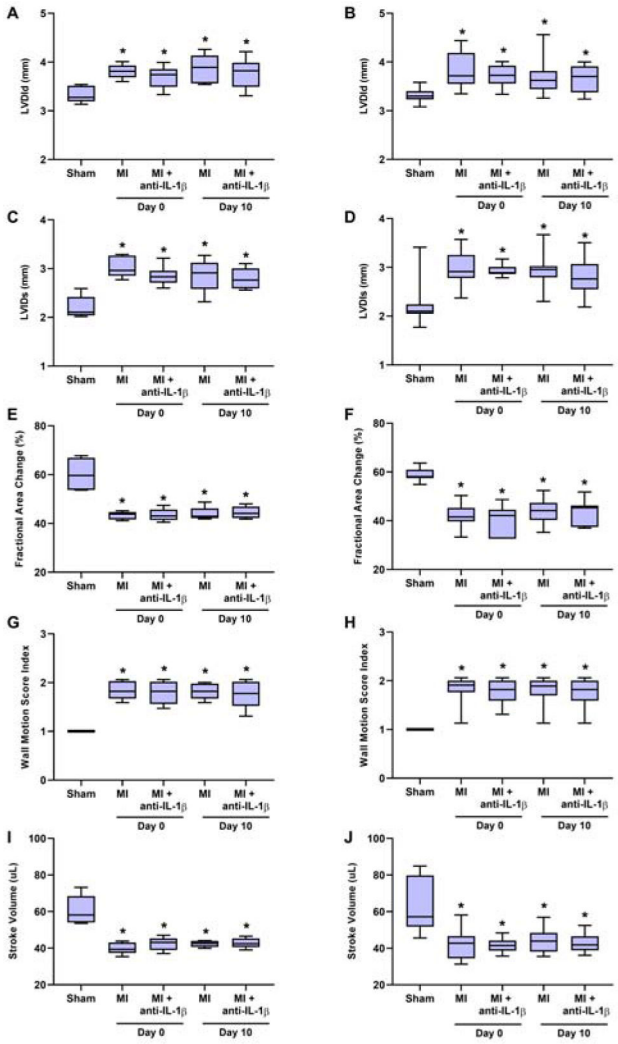

Figure 2.

Echocardiographic measurements in wild-type *left panels*) and DKO (*right panels*) mice undergoing either sham procedure or closed-chest MI. Data include LV internal diameter at end-diastole (*LVIDd*) (**A** and **B**) or end-systole (*LVIDs*) (**C** and **D**), fractional area change (**E** and **F**), wall motion score index (**G** and **H**), and stroke volume (**I** and **J**). Sham-treated animals were studied at only at day 0 based on no expected change over time. *p<0.05 vs sham-treated animals. Bar-and-whisker plots show median (bar), interquartile range (box), and range (whiskers). Number for each cohort are: wild-type: n=5 for sham and MI, n=6 for MI with anti-IL-1β therapy; DKO: n=7 for sham, n=14 for MI, n=7 for MI with anti-IL-1β therapy.

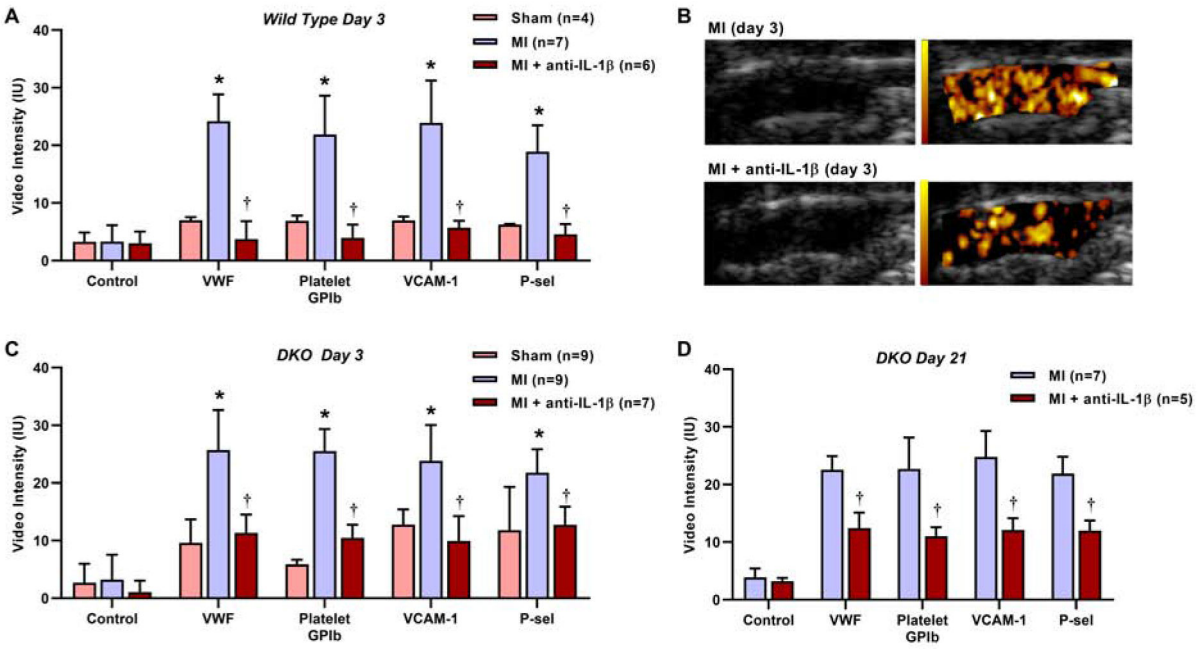

Figure 3.

Ultrasound molecular imaging data demonstrating background-subtracted intensity (mean ±SEM) obtained from the thoracic aorta for each targeted or control agent on post-MI day 3 in (**A**) wild-type and (**C**) DKO mice; and (**D**) at day 21 in DKO mice. *p<0.05 (corrected) vs sham-treated mice and vs control agent; †p<0.05 vs untreated post-MI mice. (**B**) Examples of 2-D grey-scale imaging (*left panels*) and superimposed background-subtracted color-coded (scale at left) echocardiographic molecular imaging for platelet GPIbα (*right panels*) 3 days post-MI in untreated and anti-IL1β-treated mice.

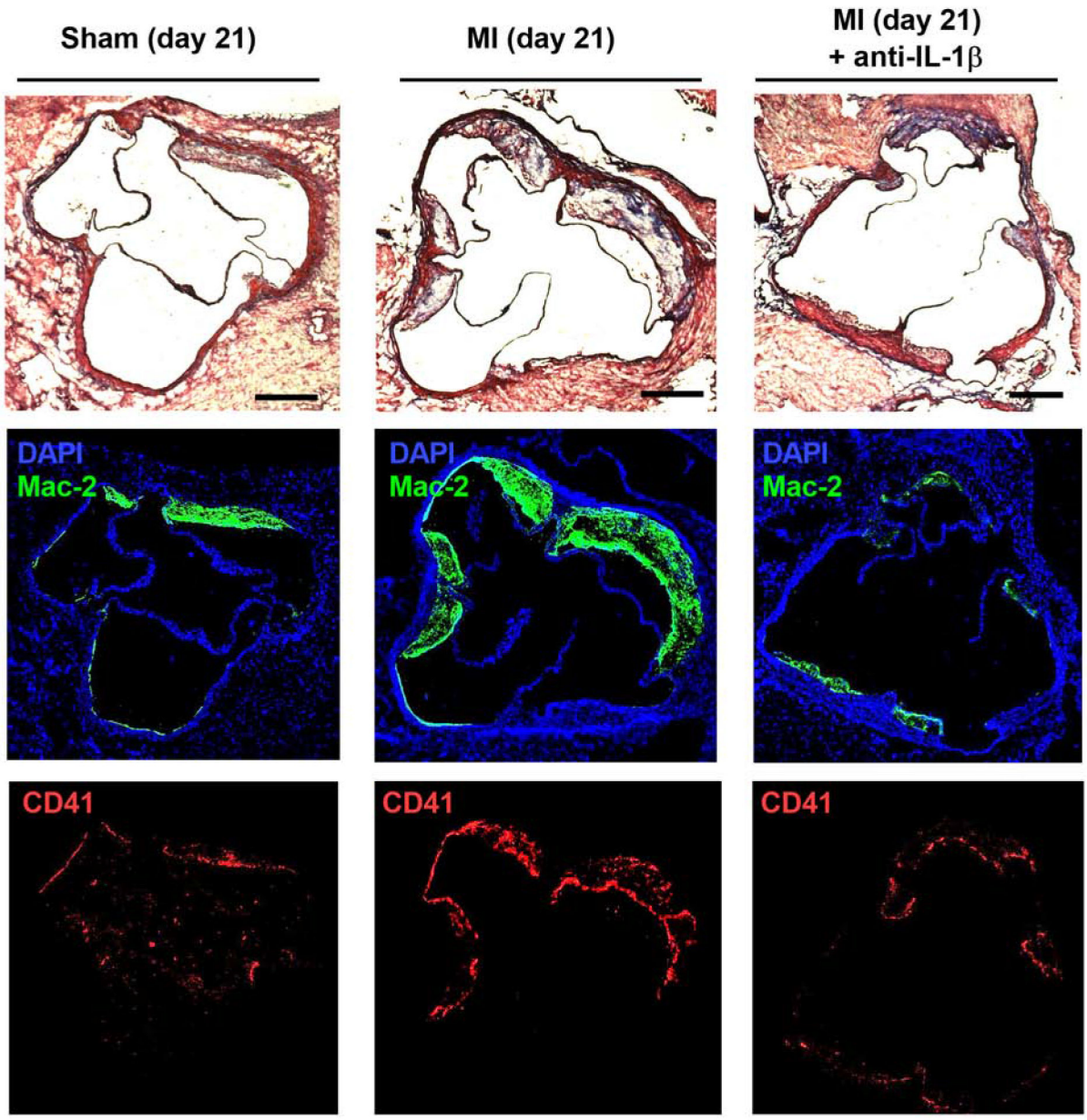

Figure 4.

Examples of histology from the aortic root of DKO mice at day 21 post-procedure in mice from the sham, MI, and MI with anti-IL-1β therapy cohorts. Masson's trichrome staining (*top*) depicts different extent of plaque formation in the aortic sinuses. Immunohistochemistry for Mac-2 (*middle*) and CD41 (*bottom*) were used to assess inflammatory status of lesions and platelet adhesion, respectively. Scale bar = 250 μm.

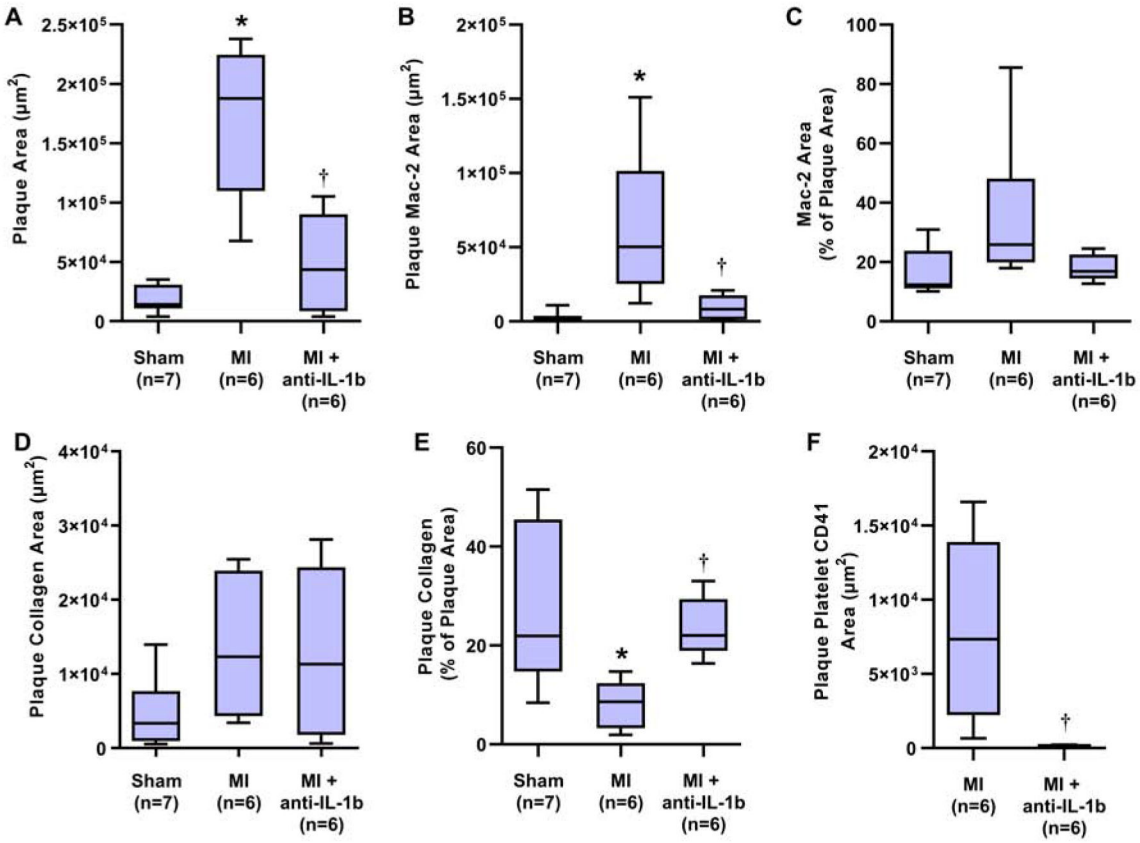

Figure 5.

Quantitative histology analysis from the aortic root showing group-wise differences between sham-treated and the post-MI DKO cohorts at 21 days. Data include (**A**) plaque area, (**B**) plaque area with positive Mac-2 staining, (**C**) percent of the plaque area with Mac-2 staining, (**D**) plaque area staining for collagen on Masson's staining, (**E**) percent of the plaque area with collagen staining, and (**F**) area staining for platelet CD41. Staining for CD41 was not normalized to plaque area based on most staining occurring on the plaque surface. *$p<0.05$ (corrected) vs sham-treated mice; †$p<0.05$ vs untreated post-MI mice.

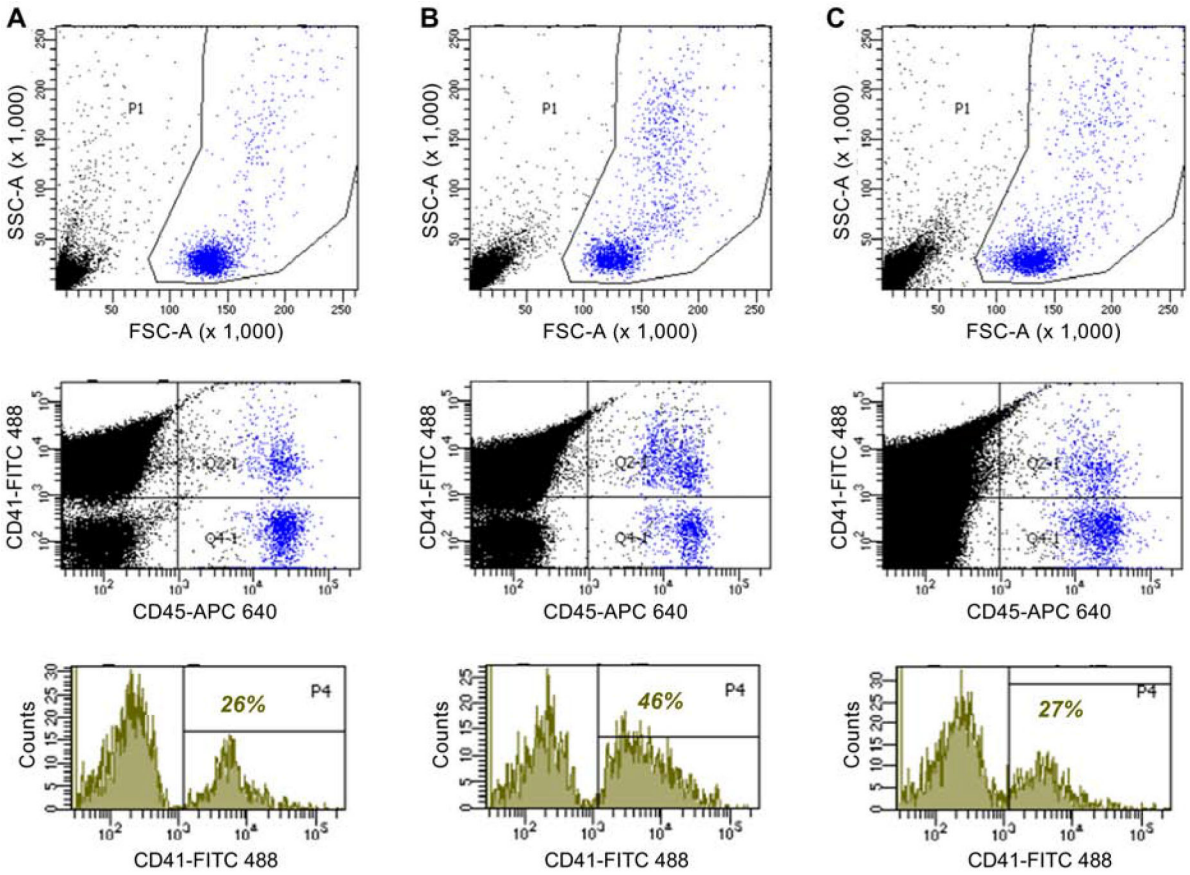

Figure 6.

Flow cytometry data for platelet-leukocyte complexes from blood samples obtained from (**A**) a control wild-type mouse, (**B**) a wild-type mouse 3 days post-MI; (**C**) a wild-type mouse treated with anti-IL-1β 3 days post-MI. The top graphs depict forward (FSC-A) versus side (SSC-A) light scatter used to draw gates around the total leukocyte population (blue events). The middle graph shows events from outside (black) and inside (blue) the leukocyte gate according to staining intensity for CD45 (APC-labeling) as a leukocyte stain, and CD41 (FITC-labeling) as a platelet stain. Events staining high for both labels were defined as platelet-leukocyte complexes. The bottom graphs show histograms of platelet staining for all events within the leukocyte gate by scatter and CD45 staining, with the percent of leukocyte events with positive CD41 staining superimposed on each graph. Control conditions are provided in Figure 2 of the on-line supplement.